Experimental characterization of microstructure development for calculating fabric and stiffness tensors in salt rock

Xianda, Shen[1], Arson, C.[1],

[1]*School of Civil and Environmental Engineering, Georgia Institute of Technology, Atlanta, Georgia*

Ding, J.[2], Chester, F. M.[2], Chester, J. S.[2]

[2]*Center for Tectonophysics, Department of Geology & Geophysics, Texas A&M University, College Station, TX 77843-3115*

ABSTRACT: Uniaxial consolidation tests were conducted on reagent-grade granular salt in dry conditions at 150 C. 2D-microscopic images, parallel to the axis of consolidation, were obtained at several stages of progressive consolidation from 15% to 3% porosity. Microstructure image analyses were performed to obtain probability density functions (PDFs) of the area, solidity, coordination number, orientation, elongation and roundness of the grains, as well as the PDFs of the branch lengths, branch orientations and solid volume fraction, defined locally over polygons with edges matching grain centroids. It is found that sample deformation is mostly due to grain rearrangement and that upon consolidation, grains become less convex, and elongate in the direction perpendicular to the loading axis. Four fabric tensors were calculated to assess microstructure anisotropy induced by grain orientation, branch length orientation, grain solidity and local solid volume fraction. Fabric tensors were diagonal and orthogonal. Therefore, their product was used to define a global fabric tensor, which was introduced in the expression of the stiffness tensors. The constitutive parameters were calibrated against the consolidation tests. The approach paves the way to enrich continuum damage and healing mechanics model with fabric descriptors that can play the role of internal variables.

1. INTRODUCTION

Salt rock is often considered as an ideal material for geological storage of compressed air and nuclear waste, because of its low permeability and favorable creep properties. Salt is a polycrystalline material made of bonded crystals (called grains in the following). Salt stiffness depends on rock microstructure, which changes during the geostorage process. A micro-macro mechanical model is proposed to predict the evolution of stiffness, deformation and microstructure development during consolidation.

A fabric tensor is a symmetric tensor that captures anisotropy due to the presence of heterogeneities in a rock. A fabric tensor can be defined in many ways to characterize the microstructure arrangement of geomaterials, and is usually regarded as the second microstructure measurement, after porosity. Crack fabric tensors were defined with space distribution, density, shape, dimension, and orientation of cracks. A fabric tensor was defined based on the density, dimension, and angular distribution of branches linking particle centers (Oda, 1982). Stereological methods were used to characterize the distribution of directional data (Kanatani, 1984). A fabric tensor can be determined by calculating the local porosity on test lines drawn in various directions of space. A set of probe lines drawn at 10° (Muhunthan and Chameau, 1997) or a set of parallel test lines in a given direction were commonly used as test lines (Kou et al. 1998). The volume fraction, the mean coordination number, and the correction factor depending on grain size distribution were found to be essential descriptors of rock microstructure, and were introduced in the trace of fabric tensors (Madadi et al., 2004).

A relationship between stiffness and fabric tensors was established, with the assumption that anisotropy was fully determined by the fabric tensor (Cowin, 1985). The model was applied to poroelasticity, considering drained and undrained conditions separately (Cowin, 2004). An elasticity model based on the fabric tensor was then proposed with two Lamé like constants only (Zysset and Curnier, 1995). A fabric tensor based on grains orientation was used to define a Drucker-Prager like yield function, taking the anisotropic yielding behavior of granular soils into account (Oda 1989).

Rock anisotropy can be due to the preferential orientation of multiple microstructure descriptors simultaneously. However, fabric tensors are usually defined to account for the orientation distribution of one descriptor only. A more global definition of fabric is needed to properly account for microstructure

development in the expression of the stiffness tensor. In this study, a continuum mechanical model is proposed to link salt stiffness to microstructure development, by means of a fabric tensor that accounts for several microstructural sources of anisotropy. Uniaxial consolidation test were conducted on reagent-grade granular salt in dry conditions at 150 C. 2D-microscopic images, parallel to the axis of consolidation, were obtained at several stages of progressive consolidation from 15% to 3% porosity. Microstructure image analyses were performed to obtain probability density functions (PDFs) of various descriptors, which are interpreted in Section 2. In Section 3, fabric tensors are calculated for selected microstructure descriptors. In Section 4, we propose a relationship between these fabric tensors and the stiffness tensor.

2. MICROSTRUCTURE DESCRIPTORS ANALYSIS

A series of consolidation tests were performed on reagent-grade granular salts in dry conditions, at 150 C. The diameter of salt particles ranged between 0.300mm and 0.355mm. The sample was 6.426cm high and 1.905cm in diameter. The tests were conducted at a constant rate of 0.034mm/s. The relation between vertical stress and vertical strain is presented in Fig.1: with the increase of vertical stress, salt exhibits higher stiffness and lower porosity.
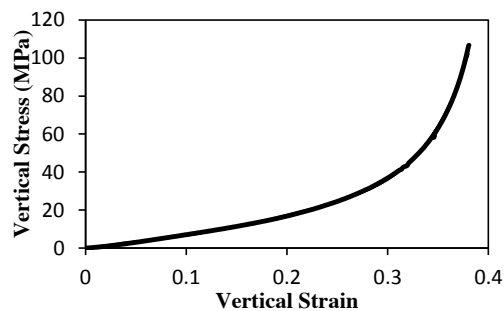
(a) Vertical stress versus vertical strain
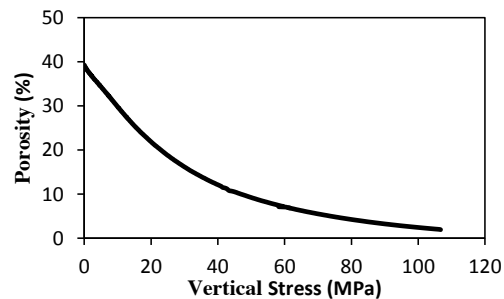
(b) Porosity versus vertical stress

Fig. 1. Consolidation test results

Microscopic images were acquired at four stages of the consolidation test, when samples reached 15%, 10%, 6% and 3% porosity (Fig.2).

(a) 3% total porosity   (b) 6% total porosity

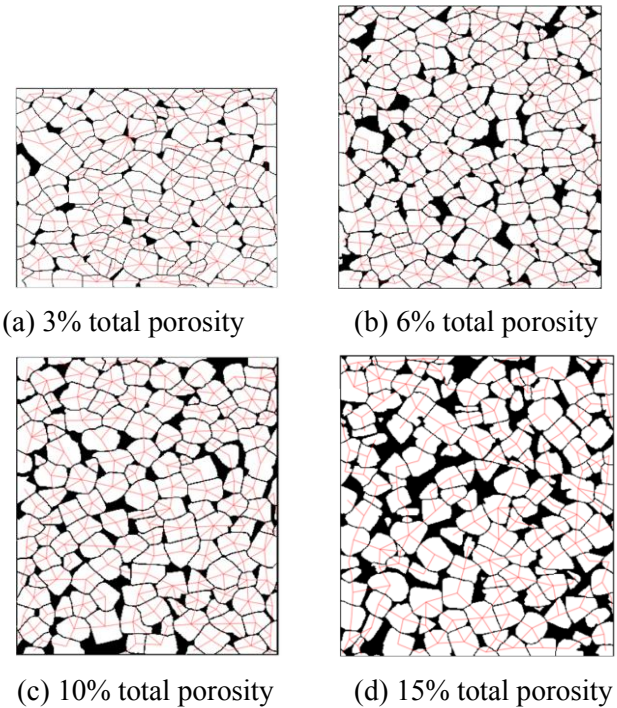(c) 10% total porosity   (d) 15% total porosity

Fig. 2. Microstructure images of salt samples (white area: salt grains, black area: voids, red lines: branches linking the centers of two grains in contact)
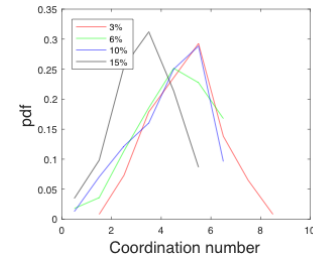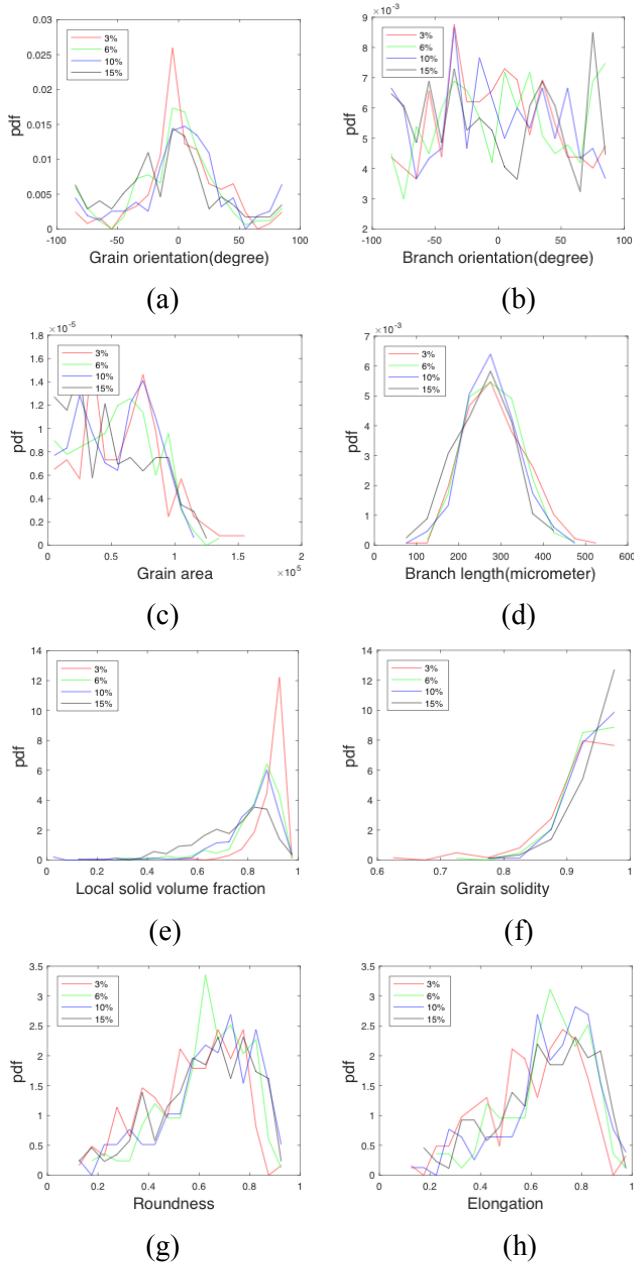
Nine microstructure descriptors were studied to characterize the evolution of microstructure during consolidation (Table 1).

Table 1. Microstructure descriptors

Descriptors	Definition
Grain orientation	Grains are represented by virtual ellipses with same second moment. The orientation is the angle between the major axis of the ellipse and the horizontal axis of the image.
Branch orientation	The angle between a branch and the horizontal axis of the image
Grain area	The area of a grain
Branch length	The length of segments linking the centroids of two grains in contact
Roundness	The ratio of the area of a particle over the area of a circle whose diameter equals to the length of the virtual ellipse's major axis
Elongation	The ratio between the minor and major axes of the virtual ellipses representing the grains
Local solid volume fraction	Solid volume fraction over a polygon with edges matching grains centroids.
Solidity	The ratio of grain area over the area

	of the grain's circumscribed circle
Coordination number	The number of grains in contact with a given grain

The probability distribution functions of the nine descriptors are presented in Fig. 3, in which 0° is the direction of horizontal axis, which is also the direction of the minimum principal stress.

(a)

(b)

(c)

(d)

(e)

(f)

(g)

(h)

(i)

Fig. 3. Probability density functions of the microstructure descriptors

According to Fig.3(a), grain orientations are initially relatively uniform, but salt grains take a preferential grain orientation under compression: the major axis of grains rotates to align with the direction of minimal principal stress. Fig. 3(b) shows branch orientations are more uniform than grain orientations throughout the consolidation process, with a slight preferential orientation parallel to the direction of the minimum principal stress.

Based on Fig.3(c), the PDFs of grain area of samples at different porosity levels are similar. The volumetric deformation of salt particles' does not seem to contribute to the overall deformation of the sample. The decrease of total volume under compression mainly results from grain reorganization and void collapse. Similar conclusions can be drawn from the distribution of branch lengths, shown in Fig.3(d). The shape of branch length's PDFs is close to a normal distribution, whose mean value is slightly lower than 300mm. The distribution of branch length does not change much during compression. As microscopic images analysis is done in 2D, a large domain would have to be imaged to have a representative description of 3D anisotropy induced by lengths or areas. Thus we will not use grain area or branch length as fabric descriptors in the following.

The PDF of local solid volume fraction is presented in Fig.3(e). Lower local solid volume fraction means larger void in a polygonal area within the image. With the compaction of the sample, local solid volume fraction increases, and the distribution of void size becomes uniform. Grain solidity, which describes grain's convexity, decreases during consolidation (Fig.3(f)): dislocations and indentations under high contact forces can explain the loss of grain convexity.

The PDFs of roundness and elongation are related: the lower the roundness, the lower the elongation (Fig.3(g) and Fig.3(h)). Roundness decreases with porosity, which indicates that grains become less spherical under the effect of high contact forces. Since the grain size distribution does not depend on porosity, we conclude that grains undergo deviatoric deformation and potentially indentation from highly stressed contacts. Fig.3(i) confirms that a decrease of porosity increases

the probability of contact between grains, and therefore, increases grains coordination number.

Based on the results presented above, we select grain orientation, branch length orientation, local solid volume fraction and solidity to characterize microstructure development during consolidation.

3. FABRIC TENSOR FORMULATION

According to Oda (1989), the fabric tensor F_{ij} is expressed as:

$$F_{ij} = \int_\Omega n_i n_j E(\Omega) d\Omega \quad (i, j = 1, 2, 3)\ldots\ldots(1)$$

where n_1, n_2, n_3 are projections of a unit vector $\boldsymbol{n}$ on the Cartesian reference coordinates; Ω is the whole solid angle corresponding to a unit sphere, and equals to 4π; $E(\Omega)$ is a probability density function.

In this research, the fabric tensor depends on 2D images analysis. As a result, equation (1) is modified into:

$$\bar{F}_{ij} = \int_\Omega n_i n_j E(\Omega) d\Omega \quad (i, j = 1, 2) \quad (2)$$

where $\bar{F}_{ij}$ is a symmetric second-rank tensor; Ω equals to 2π. θ is proposed as the inclination angle of $\boldsymbol{n}$, then, the components of $\bar{F}_{ij}$ can be obtained.

$$\bar{F}_{11} = \frac{1}{N} \sum_{t=1}^{N} \sin^2 \theta^{(t)} \quad (3)$$

$$\bar{F}_{12} = \frac{1}{N} \sum_{t=1}^{N} \sin^{(t)} \cos^{(t)} \quad (4)$$

$$\bar{F}_{22} = \frac{1}{N} \sum_{t=1}^{N} \cos^{2(t)} \quad (5)$$

where N is the total number of measurements. Based on the previous image analyses, the grain orientation fabric tensors are the following:

$$G^{03} = \begin{bmatrix} 0.2049 & 0.0313 \\ 0.0313 & 0.7951 \end{bmatrix} \quad (6)$$

$$G^{06} = \begin{bmatrix} 0.2507 & 0.0027 \\ 0.0027 & 0.7493 \end{bmatrix} \quad (7)$$

$$G^{10} = \begin{bmatrix} 0.2947 & 0.0446 \\ 0.0446 & 0.7053 \end{bmatrix} \quad (8)$$

$$G^{15} = \begin{bmatrix} 0.3389 & -0.0620 \\ -0.0620 & 0.6611 \end{bmatrix} \quad (9)$$

where G03, G06, G10, and G15 are the grain orientation tensors for samples with 3%, 6%, 10% and 15% porosity

respectively. $\bar{F}_{12}$ and $\bar{F}_{21}$ in grain orientation fabric tensors are close to 0, thus the fabric tensors can be regarded as diagonal orthogonal tensors. The difference between $\bar{F}_{11}$ and $\bar{F}_{22}$ increases when sample's porosity decreases, which indicates that during consolidation, anisotropy develops in the samples.

Similarly, branch orientation fabric tensors are calculated as follows:

$$B^{03} = \begin{bmatrix} 0.4373 & -0.0164 \\ -0.0164 & 0.5627 \end{bmatrix} \quad (10)$$

$$B^{06} = \begin{bmatrix} 0.4742 & -0.0010 \\ -0.0010 & 0.5258 \end{bmatrix} \quad (11)$$

$$B^{10} = \begin{bmatrix} 0.4687 & -0.0025 \\ -0.0025 & 0.5313 \end{bmatrix} \quad (12)$$

$$B^{15} = \begin{bmatrix} 0.5128 & -0.0109 \\ -0.0109 & 0.4872 \end{bmatrix} \quad (13)$$

Branch orientation tensors can also be regarded as diagonal orthogonal tensors. During compaction, anisotropy tends to develop, but compared to grain orientation, anisotropy brought by branch orientation is not significant.

The fabric tensors of that describe the distribution of local solid volume fraction and grain solidity are obtained as follows:

$$\bar{F}_{11} = \frac{1}{N} \sum_{t=1}^{N} \left(p^{(t)}\right)^2 \sin^2 \theta^{(t)} \quad (14)$$

$$\bar{F}_{12} = \frac{1}{N} \sum_{t=1}^{N} \left(p^{(t)}\right)^2 \sin^{(t)} \cos^{(t)} \quad (15)$$

$$\bar{F}_{22} = \frac{1}{N} \sum_{t=1}^{N} \left(p^{(t)}\right)^2 \cos^{2(t)} \quad (16)$$

For the local solid volume fraction fabric tensor, p is the local solid volume fraction of each polygon and θ is the angle between the horizontal and the line connecting a polygon's center with the image's center. For the grain solidity fabric tensor, p is the grain solidity of each grain and θ is the angle between the horizontal and the line connecting a grain's center with the image's center. Equations (17), (18), (19), (20) provide the normalized local solid volume fraction fabric tensors:

$$\alpha_l^{03^2} L^{03} = \begin{bmatrix} 0.3765 & 0.0036 \\ 0.0036 & 0.4229 \end{bmatrix} = 0.8941^2 \begin{bmatrix} 0.4710 & 0.0045 \\ 0.0045 & 0.5290 \end{bmatrix} \quad (17)$$

$$\alpha_l^{06^2} L^{06} = \begin{bmatrix} 0.3815 & -0.0020 \\ -0.0020 & 0.3126 \end{bmatrix} = 0.8331^2 \begin{bmatrix} 0.5496 & -0.0028 \\ -0.0028 & 0.4504 \end{bmatrix} \quad (18)$$

$$\alpha_l^{10^2} L^{10} = \begin{bmatrix} 0.3428 & -0.0105 \\ -0.0105 & 0.3239 \end{bmatrix} = 0.8165^2 \begin{bmatrix} 0.5142 & -0.0157 \\ -0.0157 & 0.4858 \end{bmatrix} \quad (19)$$

$$\alpha_l^{15^2} L^{15} = \begin{bmatrix} 0.3098 & -0.0114 \\ -0.0114 & 0.2622 \end{bmatrix} = 0.7563^2 \begin{bmatrix} 0.5416 & -0.0252 \\ -0.0252 & 0.4584 \end{bmatrix} \quad (20)$$

Matrices L have a unit trace. The local solid volume fraction coefficient α_l is used for normalization. As expected, α_l increases as porosity decreases during compaction: $\alpha_l^{15} = 0.7563$, $\alpha_l^{10} = 0.8165$, $\alpha_l^{06} = 0.8331$, $\alpha_l^{03} = 0.8941$. The solidity fabric tensors are given in equations (21), (22), (23), (24):

$$\alpha_s^{03^2} S^{03} = \begin{bmatrix} 0.3917 & -0.0023 \\ -0.0023 & 0.4655 \end{bmatrix} = 0.9258^2 \begin{bmatrix} 0.4570 & 0.0027 \\ 0.0027 & 0.5430 \end{bmatrix} \quad (21)$$

$$\alpha_s^{06^2} S^{06} = \begin{bmatrix} 0.4671 & -0.0019 \\ -0.0019 & 0.4136 \end{bmatrix} = 0.9384^2 \begin{bmatrix} 0.5304 & -0.0022 \\ -0.0022 & 0.4696 \end{bmatrix} \quad (22)$$

$$\alpha_s^{10^2} S^{10} = \begin{bmatrix} 0.4655 & -0.0150 \\ -0.0150 & 0.4241 \end{bmatrix} = 0.9431^2 \begin{bmatrix} 0.5233 & 0.0169 \\ 0.0169 & 0.4767 \end{bmatrix} \quad (23)$$

$$\alpha_s^{15^2} S^{15} = \begin{bmatrix} 0.4590 & 0.0092 \\ 0.0092 & 0.4409 \end{bmatrix} = 0.9486^2 \begin{bmatrix} 0.5078 & 0.0010 \\ 0.0010 & 0.4922 \end{bmatrix} \quad (24)$$

The solidity fabric tensor does not exhibit any preferential orientation. The solidity coefficient α_s decreases during compaction, which marks the decrease of grain convexity with the decrease of porosity: $\alpha_s^{15} = 0.9486$, $\alpha_s^{10} = 0.9431$, $\alpha_s^{06} = 0.9384$, $\alpha_s^{03} = 0.9258$.

4. ANISOTROPIC ELASTIC MODEL

We note that in each fabric tensor, the $\overline{F}_{12}$ component is negligible in front of the diagonal components. We thus consider that all fabric tensors are diagonal and orthogonal, and we define a normalized fabric tensor H to characterize the total anisotropy induced by grain orientation, branch orientation, distribution of local solid volume fraction, and distribution of grain solidity, as follows:

$$H^i = \gamma G^i B^i L S^i \quad (25)$$

γ is a normalizing coefficient to make tr(H) equal to 1. The second-rank fabric tensor H can be written as $kI+K$. k is a scalar, and K is a traceless second-rank tensor.

According to (Zysset, 1995), the expressions of the free energy and the stiffness tensor, as functions of k, K and the strain E, are given as:

$$\begin{aligned} \psi(E,k,K) &= a_1 I \otimes I + a_2 I \, \overline{\overline{\otimes}} \, I + a_3 K \otimes K + a_4 \left(K \, \overline{\overline{\otimes}} \, I + I \, \overline{\overline{\otimes}} \, K \right) \\ &+ a_5 K^2 \otimes K^2 + a_6 K \, \overline{\overline{\otimes}} \, K + a_7 \left(I \otimes K + K \otimes I \right) \\ &+ a_8 \left(K \otimes K^2 + K^2 \otimes K \right) + a_9 \left(I \otimes K^2 + K^2 \otimes I \right) \end{aligned} \quad (26)$$

$$\begin{aligned} D = \frac{\partial^2 \psi}{\partial E^2} &= a_1 I \otimes I + a_2 I \, \overline{\overline{\otimes}} \, I + a_3 K \otimes K + a_4 \left(K \, \overline{\overline{\otimes}} \, I + I \, \overline{\overline{\otimes}} \, K \right) \\ &+ a_5 K^2 \otimes K^2 + a_6 K \, \overline{\overline{\otimes}} \, K + a_7 \left(I \otimes K + K \otimes I \right) \\ &+ a_8 \left(K \otimes K^2 + K^2 \otimes K \right) + a_9 \left(I \otimes K^2 + K^2 \otimes I \right) \end{aligned} \quad (27)$$

in which the tensor product $\overline{\overline{\otimes}}$ is defined as following:

$$A_{ij} \, \overline{\overline{\otimes}} \, B_{kl} = \frac{1}{2} \left(A_{ik} B_{mj} + A_{kj} B_{mi} \right) \quad (28)$$

With the assumption of sample statistical homogeneity, $a_1 = \lambda_c k^2$; $a_2 = 2\mu_c k^2$; $a_3 = \lambda_c$; $a_4 = 2\mu_c k$; $c_5 = 0$ $a_5 = 0$; $a_6 = 2\mu_c$; $a_7 = \lambda_c k$; $a_8 = 0$; $a_9 = 0$. μ_c and λ_c are Lamé like constants. Considering that the salt rock Young's modulus is exponentially dependent on porosity (Turner, 1987), we propose to relate μ_c and λ_c to the local solid volume fraction and the grain solidity as follows:

$$\mu_c = \mu_o \exp(m\alpha_l + n\alpha_s) \quad (29)$$

$$\lambda_c = \lambda_o \exp(m\alpha_l + n\alpha_s) \quad (30)$$

The model is calibrated against the consolidation tests. The Oedometer modulus is used for calibration. Due to the limited test data we obtain $2\mu_o+\lambda_o$ rather than μ_o and λ_o separately. Calibrated parameters are presented in Table 2. Calibrated model trends are compared to experimental data in Fig. 4. Microstructure image analysis were done in 2D, and porosity measurements were done in 3D, thus some adjustments were necessary. For example, the porosity of one of our samples was 8% according to microstructure image analysis and only 6% based on the calculation of total solid mass and total volume of the sample. Triaxial tests and 3D microstructure images are needed to validate the model.

Table 2. Calibrated model parameters

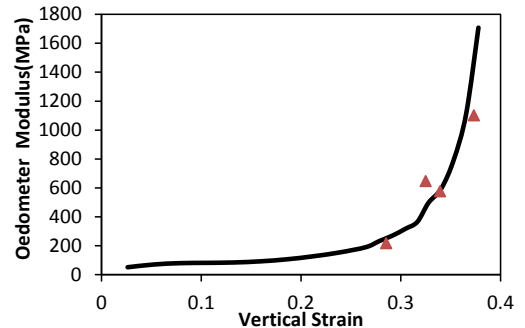| $2\mu_o+\lambda_o$ (MPa)	m	n
$3.097*10^7$	23.09	-27.63

Fig. 3. Calibration of the elastic properties (solid line: experimental results; red dots: calibrated model)

CONCLUSION

Micrographs were obtained at several stages of a uniaxial consolidation test performed on dry reagent salt at 150C. As expected, the coordination number increases during consolidation, as well as the solid volume fraction, defined locally over polygons with edges matching grains' centers. It is found that salt deformation is mostly due to grain rearrangement. During consolidation, grains elongate in the direction perpendicular to the loading axis and loose convexity, due to the probable indentation of grains in contact. Microstructure descriptors selected from 2D statistical analyses include orientation and ratios of length. Fabric tensors are calculated to assess the anisotropy induced by grain orientation, branch length orientation, distribution of local solid fraction, and distribution of solidity (i.e. grains' convexity). The four fabric tensors are diagonal and orthogonal. Therefore, their product is used to define a unique fabric tensor **H**, which indicates the overall microstructure's anisotropy. The expression of the free energy established by Zysset is used to calculate the anisotropic stiffness tensor as a function of **H**. Assuming sample's statistical homogeneity, the model depends on only two Lamé like parameters, which depend on grain solidity and solid volume fraction. The proposed constitutive model is calibrated against the consolidation tests. Results exhibit the expected trends but more experimental data is needed to validate the model, including 3D microstructure images and triaxial compression stress paths. This research provides a basis to formulate fabric-enriched continuum damage and healing models, in which the internal variables are defined as microstructure descriptors. Models will allow optimizing the healing conditions of rocks used for hosting geological storage facilities.

ACKNOWLEDGEMENTS

REFERENCES

1. Oda, M.. 1982. Fabric tensor for discontinuous geological materials. *Soil and Foundation* 22(4): 96-108.

2. Madadi, M., O. Tsoungui, M. Latzel, and S. Luding. 2004. On the fabric tensor of polydisperse granular materials in 2D. *International Journal of Solids and Structures* 41:2563–2580.

3. Muhunthan, B., and J. L. Chameau. 1997. Void fabric tensor and ultimate state surface of soils. *J. Geotech. Geoenviron*. Eng., 123(2): 173-181.

4. Kuo, C. Y., J. D. Frost and J. L. Chameau. 1998. Image analysis determination of stereology based fabric tensors. *Geotechnique* 48(4); 515-525.

5. Oda, M. and H. Nakayama. 1989. Yield function for soil with anisotropic fabric. *Journal of Engineering Mechanics* 115(1): 89-104

6. Cowin, S. C.. 1985. The relationship between the elasticity tensor and the fabric tensor. *Mechanics of Materials* 4:137-147.

7. Zysset, R.K., and A. Curnier. 1995. An alternative model for anisotropic elasticity based on fabric tensors. *Mechanics of Materials* 21:243-250.

8. Cowin, S. C.. 2004. Anisotropic poroelasticity: fabric tensor formulation. *Mechanics of Materials*. 36: 665–677.

9. Kanatani, K.. 1984. Distribution of directional data and fabric tensors. *Int. J. Engng Sci*. 22(2):149-164.

10. Turner, C. H., S. C. Cowin. 1987. Dependence of elastic constants of an anisotropic porous material upon porosity and fabric. *Journal of materials science*. 22: 3178-3184.